

## Measurements of the Proton Elastic-Form-Factor Ratio $\mu_p G_E^p/G_M^p$ at Low Momentum Transfer

G. Ron,<sup>1</sup> J. Glister,<sup>2,3</sup> B. Lee,<sup>4</sup> K. Allada,<sup>5</sup> W. Armstrong,<sup>6</sup> J. Arrington,<sup>7</sup> A. Beck,<sup>8</sup> F. Benmokhtar,<sup>9</sup> B. L. Berman,<sup>10</sup> W. Boeglin,<sup>11</sup> E. Brash,<sup>12</sup> A. Camsonne,<sup>13</sup> J. Calarco,<sup>14</sup> J. P. Chen,<sup>13</sup> Seonho Choi,<sup>4</sup> E. Chudakov,<sup>13</sup> L. Coman,<sup>15</sup> B. Craver,<sup>15</sup> F. Cusanno,<sup>16</sup> J. Dumas,<sup>17</sup> C. Dutta,<sup>5</sup> R. Feuerbach,<sup>13</sup> A. Freyberger,<sup>13</sup> S. Frullani,<sup>16</sup> F. Garibaldi,<sup>16</sup> R. Gilman,<sup>13,17</sup> O. Hansen,<sup>13</sup> D. W. Higinbotham,<sup>13</sup> T. Holmstrom,<sup>18</sup> C. E. Hyde,<sup>19,20</sup> H. Ibrahim,<sup>19</sup> Y. Ilieva,<sup>10</sup> C. W. de Jager,<sup>13</sup> X. Jiang,<sup>17</sup> M. K. Jones,<sup>13</sup> H. Kang,<sup>4</sup> A. Kelleher,<sup>18</sup> E. Khrosinkova,<sup>21</sup> E. Kuchina,<sup>17</sup> G. Kumbartzki,<sup>17</sup> J. J. LeRose,<sup>13</sup> R. Lindgren,<sup>15</sup> P. Markowitz,<sup>11</sup> S. May-Tal Beck,<sup>8</sup> E. McCullough,<sup>2</sup> D. Meekins,<sup>13</sup> M. Meziane,<sup>18</sup> Z.-E. Meziani,<sup>6</sup> R. Michaels,<sup>13</sup> B. Moffit,<sup>18</sup> B. E. Norum,<sup>15</sup> Y. Oh,<sup>4</sup> M. Olson,<sup>22</sup> M. Paolone,<sup>23</sup> K. Paschke,<sup>15</sup> C. F. Perdrisat,<sup>18</sup> E. Piasetzky,<sup>1</sup> M. Potokar,<sup>24</sup> R. Pomatsalyuk,<sup>13,25</sup> I. Pomerantz,<sup>1</sup> A. Puckett,<sup>26</sup> V. Punjabi,<sup>27</sup> X. Qian,<sup>28</sup> Y. Qiang,<sup>26</sup> R. Ransome,<sup>17</sup> M. Reyhan,<sup>17</sup> J. Roche,<sup>29</sup> Y. Rousseau,<sup>17</sup> A. Saha,<sup>13</sup> A. J. Sarty,<sup>2</sup> B. Sawatzky,<sup>15,6</sup> E. Schulte,<sup>17</sup> M. Shabestari,<sup>15</sup> A. Shahinyan,<sup>30</sup> R. Shneur,<sup>1</sup> S. Širca,<sup>24,31</sup> K. Slifer,<sup>15</sup> P. Solvignon,<sup>7</sup> J. Song,<sup>4</sup> R. Sparks,<sup>13</sup> R. Subedi,<sup>21</sup> S. Strauch,<sup>23</sup> G. M. Urciuoli,<sup>32</sup> K. Wang,<sup>15</sup> B. Wojtsekhowski,<sup>13</sup> X. Yan,<sup>4</sup> H. Yao,<sup>6</sup> X. Zhan,<sup>26</sup> and X. Zhu<sup>28</sup>

(Jefferson Lab Hall A Collaboration)

<sup>1</sup>Tel Aviv University, Tel Aviv 69978, Israel

<sup>2</sup>Saint Mary's University, Halifax, Nova Scotia B3H 3C3, Canada

<sup>3</sup>Dalhousie University, Halifax, Nova Scotia B3H 3J5, Canada

<sup>4</sup>Seoul National University, Seoul 151-747, Korea

<sup>5</sup>University of Kentucky, Lexington, Kentucky 40506, USA

<sup>6</sup>Temple University, Philadelphia, Pennsylvania 19122, USA

<sup>7</sup>Argonne National Laboratory, Argonne, Illinois 60439, USA

<sup>8</sup>NRCN, Beer-Sheva 84190, Israel

<sup>9</sup>University of Maryland, Baltimore, Maryland 20742, USA

<sup>10</sup>George Washington University, Washington, D.C. 20052, USA

<sup>11</sup>Florida International University, Miami, Florida 33199, USA

<sup>12</sup>Christopher Newport University, Newport News, Virginia, 23606, USA

<sup>13</sup>Thomas Jefferson National Accelerator Facility, Newport News, Virginia 23606, USA

<sup>14</sup>University of New Hampshire, Durham, New Hampshire 03824, USA

<sup>15</sup>University of Virginia, Charlottesville, Virginia 22904, USA

<sup>16</sup>INFN, Sezione Sanità and Istituto Superiore di Sanità, Laboratorio di Fisica, I-00161 Rome, Italy

<sup>17</sup>Rutgers, The State University of New Jersey, Piscataway, New Jersey 08855, USA

<sup>18</sup>College of William and Mary, Williamsburg, Virginia 23187, USA

<sup>19</sup>Old Dominion University, Norfolk, Virginia 23508, USA

<sup>20</sup>Université Blaise Pascal/CNRS-IN2P3, F-63177 Aubière, France

<sup>21</sup>Kent State University, Kent, Ohio 44242, USA

<sup>22</sup>Saint Norbert College, Green Bay, Wisconsin 54115, USA

<sup>23</sup>University of South Carolina, Columbia, South Carolina 29208, USA

<sup>24</sup>Institute "Jožef Stefan", 1000 Ljubljana, Slovenia

<sup>25</sup>Kharkov Institute, Kharkov 310108, Ukraine

<sup>26</sup>Massachusetts Institute of Technology, Cambridge, Massachusetts 02139, USA

<sup>27</sup>Norfolk State University, Norfolk, Virginia 23504, USA

<sup>28</sup>Duke University, Durham, North Carolina 27708, USA

<sup>29</sup>Ohio University, Athens, Ohio 45701, USA

<sup>30</sup>Yerevan Physics Institute, Yerevan 375036, Armenia

<sup>31</sup>Department of Physics, University of Ljubljana, 1000 Ljubljana, Slovenia

<sup>32</sup>INFN, Sezione di Roma, 00185 Roma, Italy

(Received 4 June 2007; published 13 November 2007)

High-precision measurements of the proton elastic form-factor ratio,  $\mu_p G_E^p/G_M^p$ , have been made at four-momentum transfer,  $Q^2$ , values between 0.2 and 0.5 GeV<sup>2</sup>. The new data, while consistent with previous results, clearly show a ratio less than unity and significant differences from the central values of several recent phenomenological fits. By combining the new form-factor ratio data with an existing cross-section measurement, one finds that in this  $Q^2$  range the deviation from unity is primarily due to  $G_E^p$  being smaller than expected.

Elastic scattering of electrons from protons reveals information about the distribution of charge and magnetism in the nucleon via the electromagnetic form factors. For decades, these form factors were determined by making Rosenbluth separations [1] of cross-section results, as done, for example, in the reanalysis by Arrington [2]. Recently, however, high-quality polarized electron beams have allowed polarization techniques [3–5] to be used. The new techniques revealed that the electric to magnetic proton form-factor ratio, which was long thought to be nearly unity for all four-momentum transfers,  $Q^2$ , becomes significantly less than unity at  $Q^2 > 1 \text{ GeV}^2$  [6]. This observation has led to a renewed experimental focus on the proton electromagnetic form factors [7–13].

A recent suggestion from a modern form-factor fit that there is structure in each of the four nucleon electromagnetic form factors for even  $Q^2 < 1 \text{ GeV}^2$  is intriguing [14] and has been discussed in recent review articles [15–17]. The interest stems from the fact that changes of just a few percent in the nucleon form factors at low  $Q^2$  have direct implications on our understanding of nucleon structure. These include, but are not limited to, the weak form factors of the nucleon [18–21], generalized parton distributions accessed in deeply virtual Compton scattering [22], generalized polarizabilities accessed in virtual Compton scattering [23], and the extraction of the Zemach radius [24].

The highest precision data set of the ratio  $\mu_p G_E^p/G_M^p$  at low  $Q^2$ , prior to the results reported herein, is from Bates BLAST [13]. This set has two out of eight points  $2\sigma$  (statistical) below unity with the average of the eight points equal to  $0.99 \pm 0.01$ . However, when systematic uncertainties are included, no point is significantly lower than  $1\sigma$  from unity, and thus it was concluded [13] that the data were consistent with unity.

In this Letter we present new, high-precision measurements of  $\mu_p G_E^p/G_M^p$  at  $Q^2$  between 0.2 and 0.5  $\text{GeV}^2$  via the polarization-transfer reaction  $^1\text{H}(\vec{e}, e'\vec{p})$ . In the Born approximation the ratio of the transferred transverse to longitudinal polarizations relates to the electromagnetic form factors through the equation:

$$R \equiv \mu_p \frac{G_E^p}{G_M^p} = -\mu_p \frac{E_e + E'_e}{2M} \tan\left(\frac{\theta_e}{2}\right) \frac{P_T}{P_L}, \quad (1)$$

where  $\mu_p$  is the proton magnetic moment,  $M$  is the mass of the proton,  $E_e$  ( $E'_e$ ) is the incident (scattered) electron energy,  $\theta_e$  is the electron scattering angle and  $P_T$  ( $P_L$ ) is the recoil proton polarization transverse (longitudinal) to the proton momentum. In this approximation the third or normal polarization component is zero.

The experiment was performed in Hall A of the Thomas Jefferson National Accelerator Facility. The polarized electrons  $\vec{e}$  were produced from a strained-superlattice GaAs crystal from the photoelectron gun [25] and were accelerated to either 362 or 687 MeV. The beam helicity state was flipped pseudorandomly at 30 Hz; beam charge

asymmetries between the two helicity states were negligible. Because of multihall running the degree of longitudinal polarization in Hall A was limited to 40% rather than the full 80%. Note from Eq. (1) that  $R$  is independent of the beam polarization, though the uncertainties do increase as a result of the lower beam polarization.

The polarized beam was incident on a 15 cm long, liquid hydrogen target. The kinematics of the measurements are given in Table I. In all cases, the elastically scattered protons were detected in the left high-resolution spectrometer (HRS), which contains a focal plane polarimeter (FPP). Six of the eight measurements were done as single-arm proton measurements, since obstructions in the Hall prevented detecting electrons at angles larger than  $60^\circ$ . In the two measurements where it was possible, the coincident scattered electrons were detected in the right HRS. Details of the standard Hall A equipment can be found in [26].

For the singles data, it was necessary to apply cuts on the target interaction position, and to subtract residual end-cap events using spectra taken on an aluminum dummy target. The two coincidence points were essentially background-free, due to the large  $ep$  cross section. Quasielastic events from the target end caps, through the  $\text{Al}(e, e'p)$  reaction, were suppressed by requiring hydrogen elastic kinematics.

For the scattered protons, the polarization precesses as the particle is transported through the spectrometer. At the FPP, the transverse polarization components lead to azimuthal asymmetries in the rescattering in the analyzing material due to spin-orbit interactions. The alignment of the FPP chambers was determined with straight-through trajectories, with the analyzing material removed. While misalignments and detector inefficiencies lead to false asymmetries, these false asymmetries largely cancel in forming the helicity differences that determine the polarization-transfer observables. The transferred polarization was determined by a maximum likelihood method using the difference of the azimuthal distributions corresponding to the two beam helicity states. The spin transport in the spectrometer was taken into account using a magnetic model calculation. Previous Hall A measurements of the form-factor ratio used the same procedures [6,7,9,11,27,28].

The form-factor ratio is determined from the ratio of polarization-transfer components, and thus from the phase shift of the azimuthal scattering distribution in the FPP analyzer. The analyzing power, efficiency, and beam polarization cancel out in the calculation of the form-factor ratio—although they affect the size of the uncertainty; thus, the main issue for systematic uncertainties is spin transport in the spectrometer. The spin-transport systematic uncertainties are determined by studying how the form-factor ratio changes when parameters such as reconstructed angles and the spectrometer bend angle are changed by their uncertainties. Detailed optical studies

TABLE I. Kinematics and FPP parameters for the measured data points. The central spin precession angle is  $\chi$ .  $\theta_{\text{lab}}^p$  and  $T_p$  are the proton lab angle and proton kinetic energy, respectively.  $S(C)$  denotes a single-arm (coincidence) measurement. The analyzer material was carbon with a density  $\approx 1.7 \text{ g/cm}^3$ .

| $Q^2(\text{GeV}^2)$ | $E_e(\text{GeV})$ | $\theta_{\text{lab}}^p(\text{deg})$ | $T_p(\text{GeV})$ | Analyzer thickness (inches) | $\chi(\text{deg})$ | $S/C$    |
|---------------------|-------------------|-------------------------------------|-------------------|-----------------------------|--------------------|----------|
| 0.225               | 0.362             | 28.3                                | 0.120             | 0.75                        | 91.0               | <i>S</i> |
| 0.244               | 0.362             | 23.9                                | 0.130             | 0.75                        | 91.9               | <i>S</i> |
| 0.263               | 0.362             | 18.8                                | 0.140             | 0.75                        | 92.7               | <i>S</i> |
| 0.277               | 0.362             | 14.1                                | 0.148             | 0.75                        | 93.4               | <i>S</i> |
| 0.319               | 0.687             | 47.0                                | 0.170             | 2.25                        | 95.3               | <i>C</i> |
| 0.356               | 0.687             | 44.2                                | 0.190             | 3.75                        | 97.0               | <i>C</i> |
| 0.413               | 0.687             | 40.0                                | 0.220             | 3.75                        | 99.6               | <i>S</i> |
| 0.488               | 0.687             | 34.4                                | 0.260             | 3.75                        | 103.0              | <i>S</i> |

were performed to constrain the spin transport for the first Hall A  $G_E^p$  experiment [6], which had the FPP mounted in HRS-right. The FPP was moved to HRS-left for the second  $G_E^p$  experiment [9] and has remained there for subsequent experiments, but no similarly detailed optical studies have been performed. As the spectrometers are nearly identical, it is expected that the limiting systematic uncertainties in this measurement are similar, though since we lack the optical studies for HRS-left, our estimated systematic uncertainties are twice as large.

To control the systematics in this experiment, each polarization point was measured at three different spectrometer momentum settings, spaced 2%–3% apart. In all cases, the polarization values extracted were consistent for the three settings. The uncertainties resulting from the subtraction of residual Al end-cap events were negligible compared with the other systematic uncertainties. The kinematics of the reaction are well determined by the recoil proton; thus, there is no discernible improvement in the uncertainties when performing a coincidence measurement. The benefit of the coincidence trigger is the suppression of background events, which for a fixed data-acquisition rate allowed for higher statistics within a shorter time.

The experimental results are summarized in Table II. The average FPP analyzing power  $\langle A_c \rangle$  and efficiency  $\varepsilon_{\text{FPP}}$  are consistent with parametrizations of earlier FPP results [29]. The Hall A FPP design allows a much broader angular acceptance than many previous devices, usually limited to about  $20^\circ$ , which leads to a slightly larger efficiency. Also, at the lowest energies, the analyzing power increases at angles beyond  $20^\circ$ , leading to a somewhat larger average analyzing power. The analyzing power quoted is the rms result, so that the FPP figure of merit (FOM) is given by  $\varepsilon_{\text{FPP}} \langle A_c \rangle^2$ .

The new data, along with other high-precision results, are shown in Fig. 1 with the four data points taken at 362 MeV beam energy having been combined into a single point for plotting. Included in the figure are a representative sample of the numerous modern calculations and fits that are available. The high statistical precision points at

$Q^2 = 0.356$  and  $0.413 \text{ GeV}^2$  clearly indicate that  $R < 1$ . While the BLAST data alone were consistent with unity [13], usually at the upper end of the uncertainty, the BLAST data are also consistent with the new measurements, and the combination of the two data sets is clearly not consistent with unity. The point at  $0.356 \text{ GeV}^2$  is  $5\sigma(\text{stat.} + \text{syst.})$  below unity and the point at  $0.413 \text{ GeV}^2$  is  $3.4\sigma$  below unity; previous data were within  $\sim 2\sigma(\text{stat.})$  of unity.

Although a smooth falloff of  $\mu_p G_E^p/G_M^p$  with  $Q^2$  is not ruled out, the new data hint at a local minimum in the form-factor ratio at about  $0.35\text{--}0.4 \text{ GeV}^2$ . Assuming uncorrelated uncertainties, in the range  $Q^2 = 0.3\text{--}0.45 \text{ GeV}^2$ , we find the world data including the current work average to  $0.960 \pm 0.005 \pm 0.005$ . This is  $3\sigma$  lower than the neighboring  $Q^2$  range  $0.45\text{--}0.55 \text{ GeV}^2$ , where  $R = 0.987 \pm 0.005 \pm 0.006$ . In this latter range, the form-factor ratio is only  $1.6\sigma$  below unity. Calculations that tend to agree with the new ratio results, such as the light-front cloudy-bag model calculation by Miller [30], however, show a monotonic decrease of the form-factor ratio. Additional calculations may be found in [11].

By combining the present measurement with previous cross-section results, it is possible to extract the individual form factors. This was done by combining the highest precision existing cross-section data in the vicinity of the

TABLE II. Shown are the experimental ratio results with statistical and systematic uncertainties along with the FPP analyzing power  $\langle A_c \rangle$  and efficiency  $\varepsilon_{\text{FPP}}$  for a secondary scattering angle range of  $5^\circ$  to  $40^\circ$ .

| $Q^2(\text{GeV}^2)$ | $\langle A_c \rangle$ | $\varepsilon_{\text{FPP}}(\%)$ | FOM (%) | $R \pm \text{stat.} \pm \text{sys.}$ |
|---------------------|-----------------------|--------------------------------|---------|--------------------------------------|
| 0.225               | 0.16                  | 1.17                           | 0.03    | $0.9570 \pm 0.0857 \pm 0.0036$       |
| 0.244               | 0.22                  | 1.03                           | 0.05    | $0.9549 \pm 0.0500 \pm 0.0037$       |
| 0.263               | 0.24                  | 1.04                           | 0.06    | $1.0173 \pm 0.0495 \pm 0.0035$       |
| 0.277               | 0.30                  | 1.00                           | 0.09    | $1.0060 \pm 0.0504 \pm 0.0030$       |
| 0.319               | 0.34                  | 6.05                           | 0.70    | $0.9691 \pm 0.0143 \pm 0.0058$       |
| 0.356               | 0.36                  | 6.94                           | 0.90    | $0.9441 \pm 0.0099 \pm 0.0050$       |
| 0.413               | 0.46                  | 4.73                           | 1.00    | $0.9491 \pm 0.0138 \pm 0.0053$       |
| 0.488               | 0.46                  | 4.73                           | 1.00    | $0.9861 \pm 0.0189 \pm 0.0094$       |

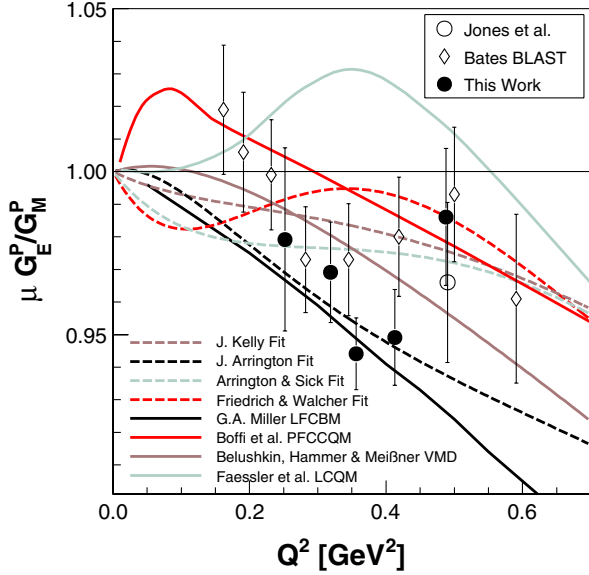


FIG. 1 (color online). The proton form-factor ratio as a function of four-momentum transfer  $Q^2$  shown with world data with total uncertainties below 3% [6,13]. The dotted and dash-dotted lines are fits [2,14,38,39], while the dashed and solid lines are from a vector-meson dominance calculation [32], light-front cloudy-bag model calculation [30], a light-front quark model calculation [40], and a point-form chiral constituent quark model calculation [41].

measured ratio [31] at  $Q^2 = 0.389 \text{ GeV}^2$  with the average of our form-factor ratios from  $Q^2 = 0.36$  and  $0.41 \text{ GeV}^2$ . Figure 2, which uses the same codes as Fig. 1, shows that the form-factor extraction is essentially independent of  $\varepsilon$ , the virtual photon polarization, over the extracted range. Interestingly, the deviation from unity in the ratio seems to be dominated by the electric form factor. This result is consistent with previous Rosenbluth separation measurements and fits in this region of  $Q^2$ ; the Rosenbluth results tend to have  $\sim 1\%$ – $3\%$  uncertainties for each of the form factors, while the fits vary by several percent for each [2]. While the Belushkin *et al.* calculation [32] generally fits best over the full  $Q^2$  range of this measurement, and at  $Q^2 = 0.389 \text{ GeV}^2$  is closest to  $G_E^p$ , it overpredicts  $R$  by underestimating  $G_M^p$ . The best fit of the ratio at  $Q^2 = 0.389 \text{ GeV}^2$  is from Arrington [2], which overpredicts each form factor by  $1\%$ – $2\%$ . The Miller calculation predicts the ratio at  $Q^2 = 0.389 \text{ GeV}^2$  well, but also overpredicts each form factor by about  $1\%$ – $2\%$ . In fact, none of these modern calculations predicts both the individual form factors and the ratio correctly. Some calculations, which were not shown, such as the light-front constituent quark model by Cardarelli *et al.* [33], are in good agreement with the form-factor ratio data in this  $Q^2$  range, but the individual form factors are significantly overestimated by present quark potential models [34].

The comparison of fits with the new data suggests that a critical reexamination is needed of experiments (e.g.,

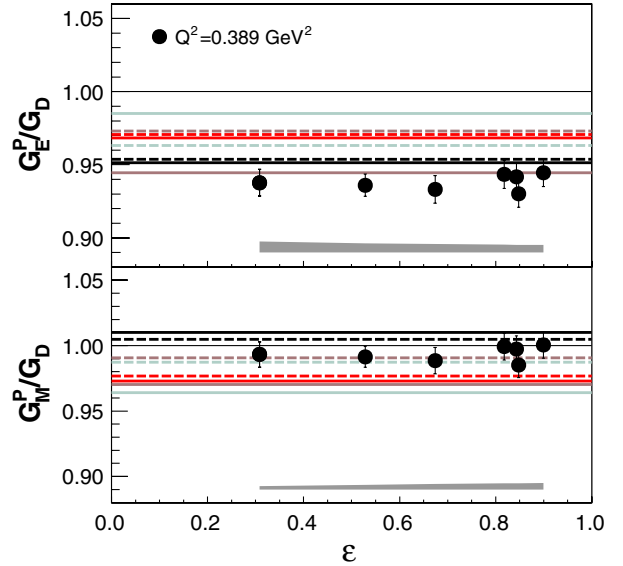


FIG. 2 (color online). The extracted individual proton form factors as a function of  $\varepsilon$ . The form factors were obtained for a single  $Q^2$  value using the average of the  $0.356$  and  $0.413 \text{ GeV}^2$  data of this work and existing cross-section data at  $0.389 \text{ GeV}^2$  [31]. The error bars indicate the statistical error of the Berger *et al.* data while the shaded region indicates how the uncertainty on the asymmetry shifts the points. The systematic uncertainty of the cross-section experiment, approximately 2% on each form factor, have not been included. The lines are the same as in Fig. 1.

[20,22,35]) that require a knowledge of low  $Q^2$  form factors to a precision of better than  $\sim 3\%$ . For example, for the HAPPEX measurement of the weak form factors [36] the new data adjust the measured asymmetry by about  $-0.5 \text{ ppm}$ , corresponding to a smaller effect from strange quarks, on data with a statistical uncertainty of  $\sim 1 \text{ ppm}$ . More significantly, this new result would shift the expected HAPPEX-III result [37] by 1 standard deviation.

In summary, we made polarization-transfer measurements to precisely determine the proton form-factor ratio at low  $Q^2$ . We showed that the form-factor ratio differs from unity at low  $Q^2$  and that the deviation is most likely dominated by the electric form factor. Our data suggest a lower value of the ratio and electric form factor than many modern fits. No fit or calculation adequately represents the ratio and extracted form-factor data over the entire range.

We thank the Jefferson Lab physics and accelerator divisions for their support. This work was supported by the U.S. Department of Energy, the U.S. National Science Foundation, Argonne National Laboratory under Contract No. DE-AC02-06CH11357, the Israel Science Foundation, the Korea Research Foundation, the U.S.-Israeli Bi-National Scientific Foundation, and the Adams Fellowship Program of the Israel Academy of Sciences and Humanities. Jefferson Science Associates operates the Thomas Jefferson National Accelerator Facility under

DOE Contract No. DE-AC05-06OR23177. The polarimeter was funded by the U.S. National Science Foundation, Grants No. PHY 9213864 and No. PHY 9213869.

- 
- [1] M. N. Rosenbluth, Phys. Rev. **79**, 615 (1950).  
[2] J. Arrington, Phys. Rev. C **69**, 032201(R) (2004).  
[3] A. I. Akhiezer, L. N. Rozentsweig, and I. M. Shmushkevich, Sov. Phys. JETP **6** (1958).  
[4] N. Dombey, Rev. Mod. Phys. **41**, 236 (1969).  
[5] R. G. Arnold, C. E. Carlson, and F. Gross, Phys. Rev. C **23**, 363 (1981).  
[6] M. K. Jones *et al.*, Phys. Rev. Lett. **84**, 1398 (2000).  
[7] O. Gayou *et al.*, Phys. Rev. C **64**, 038202 (2001).  
[8] T. Pospischil *et al.*, Eur. Phys. J. A **12**, 125 (2001).  
[9] O. Gayou *et al.*, Phys. Rev. Lett. **88**, 092301 (2002).  
[10] I. A. Qattan *et al.*, Phys. Rev. Lett. **94**, 142301 (2005).  
[11] V. Punjabi *et al.*, Phys. Rev. C **71**, 055202 (2005).  
[12] M. K. Jones *et al.*, Phys. Rev. C **74**, 035201 (2006).  
[13] C. B. Crawford *et al.*, Phys. Rev. Lett. **98**, 052301 (2007).  
[14] J. Friedrich and T. Walcher, Eur. Phys. J. A **17**, 607 (2003).  
[15] C. E. Hyde-Wright and K. de Jager, Annu. Rev. Nucl. Part. Sci. **54**, 217 (2004).  
[16] C. F. Perdrisat, V. Punjabi, and M. Vanderhaeghen, Prog. Part. Nucl. Phys. **59**, 694 (2007).  
[17] J. Arrington, C. D. Roberts, and J. M. Zanotti, J. Phys. G **34**, S23 (2007).  
[18] A. Acha *et al.*, Phys. Rev. Lett. **98**, 032301 (2007).  
[19] K. A. Aniol *et al.*, Phys. Rev. Lett. **82**, 1096 (1999).  
[20] D. S. Armstrong *et al.*, Phys. Rev. Lett. **95**, 092001 (2005).  
[21] F. E. Maas *et al.*, Phys. Rev. Lett. **94**, 152001 (2005).  
[22] C. Munoz Camacho *et al.*, Phys. Rev. Lett. **97**, 262002 (2006).  
[23] J. Roche *et al.* (VCS), Phys. Rev. Lett. **85**, 708 (2000).  
[24] I. Sick, Phys. Lett. B **576**, 62 (2003).  
[25] M. L. Stutzman *et al.*, Nucl. Instrum. Methods Phys. Res., Sect. A **574**, 213 (2007).  
[26] J. Alcorn *et al.*, Nucl. Instrum. Methods Phys. Res., Sect. A **522**, 294 (2004).  
[27] S. Strauch *et al.*, Phys. Rev. Lett. **91**, 052301 (2003).  
[28] B. Hu *et al.*, Phys. Rev. C **73**, 064004 (2006).  
[29] M. W. McNaughton *et al.*, Nucl. Instrum. Methods Phys. Res., Sect. A **241**, 435 (1985).  
[30] G. A. Miller, Phys. Rev. C **66**, 032201(R) (2002).  
[31] C. Berger, V. Burkert, G. Knop, B. Langenbeck, and K. Rith, Phys. Lett. **35B**, 87 (1971).  
[32] M. A. Belushkin, H. W. Hammer, and U.-G. Meissner, Phys. Rev. C **75**, 035202 (2007).  
[33] F. Cardarelli and S. Simula, Phys. Rev. C **62**, 065201 (2000).  
[34] S. Simula (private communication).  
[35] V. Nazaryan, C. E. Carlson, and K. A. Griffioen, Phys. Rev. Lett. **96**, 163001 (2006).  
[36] K. A. Aniol *et al.*, Phys. Rev. C **69**, 065501 (2004).  
[37] K. Paschke *et al.*, Jefferson Lab Experiment No. E05-109, 2005.  
[38] J. J. Kelly, Phys. Rev. C **70**, 068202 (2004).  
[39] J. Arrington and I. Sick, Phys. Rev. C **76**, 035201 (2007).  
[40] A. Faessler, T. Gutsche, V. E. Lyubovitskij, and K. Pumsard, Phys. Rev. D **73**, 114021 (2006).  
[41] S. Boffi *et al.*, Eur. Phys. J. A **14**, 17 (2002).